A Novel Hybrid Active Noise Control System for Composite Disturbance Signal

Chenyang Ji[1], Yizhou Gong[1], Yang Wang[1]
[1]School of Information Science and Technology, ShanghaiTech University, Shanghai, China
{jichy2024, gongyzh2022, wangyang4}@shanghaitech.edu.cn

***Abstract*—This paper presents a novel hybrid active noise control (ANC) system designed to effectively mitigate a certain class of composite noise, characterized by the superposition of broadband noise and periodic signals at certain distinct frequencies with relatively high amplitudes. The proposed method leverages the strengths of the filtered-x least mean square (LMS) algorithm, which is highly effective at suppressing broadband noise. To further enhance performance, a switching mechanism is introduced that integrates the concept of internal model control (IMC) to address the inherent limitations of the LMS algorithm, such as the waterbed effect and its inability to effectively handle periodic disturbances at specific frequencies. Experimental results, including a comprehensive comparative analysis using an ANC verification platform, demonstrate the superior noise attenuation capabilities of the proposed approach and highlight its promising potential for practical applications in environments with complex and mixed noise profiles.**

***Index Terms*—Active noise control, composite noise, internal model, switching mechanism.**

I. Introduction

Active noise control (ANC) has become a widely applied noise reduction technique in both industrial and everyday environments in recent years, particularly for addressing mid- to low-frequency noise that passive noise control cannot effectively handle. The pioneering works date back to around 1985 [1], and the field has been extensively studied since the mid-1990s [2], [3]. Despite the achievements so far, there are still significant limitations when addressing *broadband acoustic sources*, especially in industrial applications such as vehicle interiors and construction sites, where the noise is typically characterized by the superposition of broadband white noise from the environment and periodic signals generated by rotating machines [4]–[6].

The widely recognized filtered-x least mean square (FxLMS) algorithm is known for its ease of implementation and effectiveness in broadband noise cancellation [7]–[12]. However, a significant limitation is the 'waterbed effect' [13]–[15], where achieving noise reduction performance (NRP) at certain frequencies within a feedback ANC system can inadvertently increase noise levels at other frequencies. This issue often requires recalibration or redesign of ANC systems for specific applications, making it impractical to develop a universally high-NRP filtered-based ANC across all frequencies. Furthermore, these techniques typically struggle to achieve high-NRP for periodic noise at specific frequencies, with limited attenuation of approximately -10 to -20 dB [16]. Alternatively, internal model (IM)-based control [17]–[19] offers a solution for disturbance cancellation by using a replica of the exosystem to generate anti-noise signals, effectively canceling disturbances at targeted frequencies. Despite this, the limitations of both approaches emphasize the need for a more comprehensive noise suppression solution.

Based on above observations, we propose a novel hybrid IMC-LMS controller, that combines the IM-based control and feedback-type FxLMS through a novel switching mechanism. The proposed controller mitigates the waterbed effect and simultaneously suppresses both low-frequency sinusoidal noise and broadband components. Furthermore, the potential stability risks associated with individual algorithms are avoided due to the integration of the switching mechanism. The main contributions of this paper are summarized as follows:

i) We propose a 2-DOF ANC architecture with a novel switching mechanism, achieving significant NRP for broadband noise while overcoming the waterbed effect;
ii) The proposed method was validated on an acoustic duct ANC platform, and its robustness and adaptability in the presence of abrupt noise changes were demonstrated through comparative experiments;
iii) We decompose the noise into broadband components and periodic disturbances, treating them independently, which allows the method to achieve efficient frequency domain resource allocation. This approach facilitates an optimal trade-off between convergence speed and steady-state error, underscoring its superior performance in dynamic noise environments.

II. Problem Formulation

This paper employs an acoustic duct ANC system that has been widely used as a test bench for ANC algorithms [20] to reveal the core idea and effectiveness of the proposed method. Fig. 1 illustrates the components of a standard acoustic duct ANC system which depicts two distinct paths: the *Primary Path* from noise loudspeaker to error microphone, and the *Secondary Path* from anti-noise loudspeaker to error microphone. In this work, we focus on a feedback structure without a reference microphone. Specifically, the noise source (denoted as $\bar{d}(n)$) composed of low-frequency sinusoidal signals and broadband white noise, undergoes processing through the

This work was supported in part by the Yangfan Program of Shanghai, China, under Grant 21YF1429600. Corresponding author: Y. Wang.

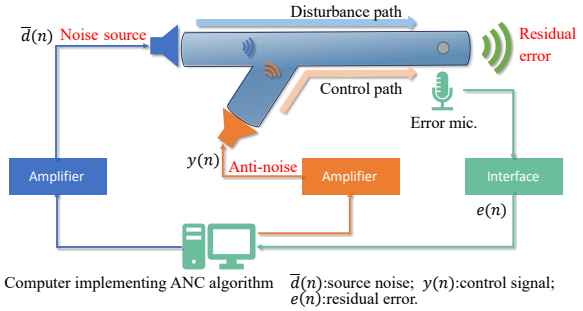

Fig. 1. The standard ANC system without a reference microphone.

primary path $P(z)$ and transforms into the primary noise to be eliminated, referred to as $d(n)$. The control signal, denoted as $y(n)$, needs to traverse the secondary path $S(z)$ before reaching the cancellation point to attenuate the primary noise. The strategically positioned error microphone at the open end of the system collects residual noise denoted as $e(n)$, providing essential feedback information for control design. Our goal is to devise the control signal $y(n)$ to minimize the amplitude of the error signal $e(n)$:

$$e(n) = d(n) - u(n),$$

where the anti-noise $u(n)$ is obtained by convolution $y(n)$ with the impulse response $s(n)$ of the secondary path, i.e., $s(n) * y(n)$.

III. Hybrid IMC-LMS Controller Design

The overall control architecture is depicted in Fig 2, from which the anti-noise signal $u(n)$ is decomposed into two components — $u_f(n)$ generated by the FxLMS algorithm and $u_i(n)$ produced by the IMC algorithm. Signals $u_f(n)$ and $u_i(n)$ processing through the secondary path, can be expressed as:

$$u_f(n) = y_f(n) * s(n), \quad u_i(n) = y_i(n) * s(n), \tag{1}$$

where $y_f(n)$ and $y_i(n)$ represent the outputs from the FxLMS module and the IMC module in Fig 2, respectively. Alternatively, we can express the error signal as:

$$e(n) = d(n) - s(n) * (y_f(n) + y_i(n)). \tag{2}$$

At the system architecture level, the proposed 2-DOF control algorithm integrates four core functional modules: the feedback FxLMS controller (serving as the inner loop), the outer loop IMC, a discrete notch filter module, and a mode-switching module. Importantly, the inner and outer loop controllers do not simply operate in parallel. Instead, they dynamically switch based on designed performance indexes through the mode-switching mechanism, ensuring stable and efficient noise cancellation across various noise conditions.

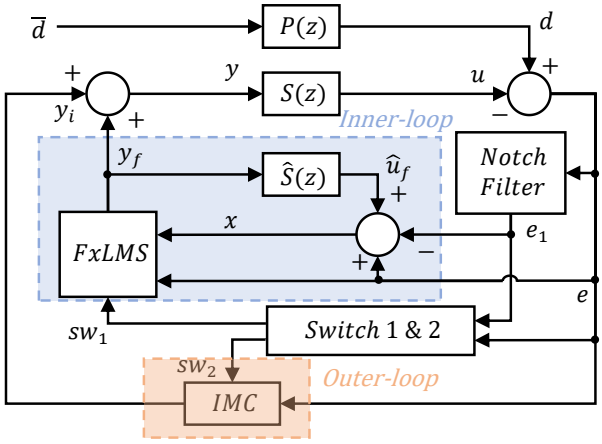

Fig. 2. The 2-DOF control block diagram the proposed algorithm.

A. The Inner-loop Controller

The objective of the inner loop controller is to reduce broadband noise. Hence, in the design of FxLMS, the reference signal $x(n)$ is obtained by filtering out the low-frequency sinusoidal component from $e(n)$:

$$x(n) = e(n) + \hat{u}_f(n) - e_1(n),$$

where $\hat{u}_f(n)$ represents the output of the inner loop $y_f(n)$ after passing through the estimated secondary path $\hat{S}(z)$ (with the corresponding impulse response defined as $\hat{s}(n)$). We employ a notch filter module to extract the periodic disturbance component $e_1(n)$ from the error signal $e(n)$. The systematic design procedures of $e_1(n)$ are given in Section III-C.

The rest design of FxLMS is standard. Denote the weight vector of the inner loop controller by $\mathbf{w}(n)$ and its filter length by N. Then, the reference vector $\mathbf{x}(n)$ and the secondary vector $\mathbf{x}_f(n)$ are given in what follows:

$$\mathbf{x}(n) = [x(n), x(n-1), \ldots, x(n-N+1)]^\top,$$
$$\mathbf{x}_f(n) = [x_f(n), x_f(n-1), \ldots, x_f(n-N+1)]^\top,$$

where $x_f(n) = x(n) * \hat{s}(n)$. The next step is critical: we utilize a switching signal $sw_1(n)$ to decide whether the adaptation law for the weight vector updates or not:

$$\mathbf{w}(n+1) = \begin{cases} \mathbf{w}(n) + \mu e(n)\mathbf{x}_f(n), & \text{if } sw_1(n) = 1 \\ \mathbf{w}(n), & \text{else} \end{cases} \tag{3}$$

where its initial value is chosen to be $\mathbf{w}(0) = \mathbf{0} \in \mathbb{R}^N$, and $\mu > 0$ represents the adaptation gain for the algorithm update. The design of switching signal $sw_1(n)$ and its logic are given in Section III-D.

Finally, the output $y_f(n)$ of the inner loop controller can be derived from the following equation:

$$y_f(n) = \mathbf{w}^\top(n)\mathbf{x}(n). \tag{4}$$

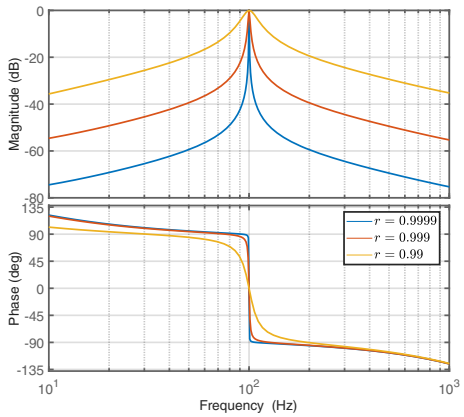

Fig. 3. The Bode plot of the notch filter over various values of r.

B. The Outer-loop Controller

To cancel the low-frequency sinusoidal component, we present an IMC in [17] as the outer loop controller:

$$\begin{aligned}\hat{\eta}_1(n+1) =& \hat{\eta}_2(n) + gR_\omega(\cos\omega)e_1(n),\\ \hat{\eta}_2(n+1) =& -\hat{\eta}_1(n) + 2(\cos\omega)\hat{\eta}_2(n) - gR_\omega e_1(n),\\ y_i(n) =& \begin{cases} -\hat{\eta}_1(n) - gR_\omega e_1(n), & \text{if } sw_2(n)=1\\ 0, & \text{else}\end{cases}\end{aligned} \tag{5}$$

where the tuning gain $g > 0$ is sufficiently small, and R_ω represents the real part of the frequency response of $S(z)$ over frequency ω of interest. The switching signal $sw_2(n)$ decides whether the outer-loop controller is activated or not, and its design can be found in Section III-D.

C. Discrete Notch Filter

We utilize a discrete-time notch filter to obtain the filtered low-frequency sinusoidal component from $e(n)$:

$$\begin{aligned}\hat{x}(n+1) =& \begin{bmatrix} 0 & -r^2 \\ 1 & 2r\cos\omega \end{bmatrix}\hat{x}(n) + \begin{bmatrix} r^2-1 \\ 2\cos\omega(1-r)\end{bmatrix}e(n),\\ e_1(n) =& \begin{bmatrix} 0 & 1 \end{bmatrix}\hat{x}(n)\end{aligned} \tag{6}$$

where Bode plot for several values of the tuning gain r satisfying $0 < r < 1$ is shown in Fig. 3. As r approaches 1, the amplitude and phase of the periodic disturbance $e_1(n)$ increasingly approximate that of $e(n)$ over the corresponding frequency.

D. Switching Mechanism

We proceed with the design of the switching mechanism:

1) Switch to update of weight vector of inner-loop controller: Define $e_0(n) := e(n) - e_1(n)$ and the performance index as $J_1(n) = \sum_{\tau=n-L}^{n} e_0^2(\tau) + a_1 e^{-b_1 n}$, where L, a_1, and b_1 are positive tuning parameters. Note that, $e_0(n)$ is the broadband component of $e(n)$. If its integral over a time interval is larger than a upper threshold, denoted by δ_1, we activate the inner-loop controller. To avoid the wrong switch at the initial instant, we add an exponential decaying bias term in $J_1(n)$. Additionally, to ensure the system has re-initialization capability for the switching signal, another upper threshold δ_2 satisfying $\delta_1 < \delta_2$. In summary, $sw_1(n)$ is designed as

$$sw_1(n+1) = \begin{cases} 1, & \text{if } J_1(n) \geq \delta_1 \text{ and } sw_1(n) = 1\\ 0, & \text{if } J_1(n) < \delta_1 \text{ and } sw_1(n) = 1\\ 1, & \text{if } J_1(n) \geq \delta_2 \text{ and } sw_1(n) = 0\\ 0, & \text{if } J_1(n) < \delta_2 \text{ and } sw_1(n) = 0\end{cases} \tag{7}$$

2) Switch to activate the output of outer-loop controller: Similarly, we define $J_2(n) = \sum_{\tau=n-L}^{n} e_1^2(\tau) + a_2 e^{-b_2 n}$, where $e_1(n)$ is the filtered low-frequency sinusoidal component, and L, a_2, and b_2 are parameters we set. If the integral of $e_1(n)$ over a time interval is larger than a upper threshold, the IMC is activated. Hence, $sw_2(n)$ is proposed as

$$sw_2(n+1) = \begin{cases} 1, & \text{if } J_2(n) \geq \delta_3 \text{ and } sw_1(n) = 0\\ 0, & \text{else}\end{cases} \tag{8}$$

As depicted in Fig. 4, we present the flowchart of the IMC-LMS algorithm, encompassing the primary procedures of initialization, decision-making, FxLMS adaptation, IMC initiation along with the switching mechanisms and performance indexes incorporated within this framework. When $sw_1(n)$ or $sw_2(n)$ is configured to 1 or 0, it signifies the activation or deactivation of the corresponding LMS algorithm or IMC algorithm.

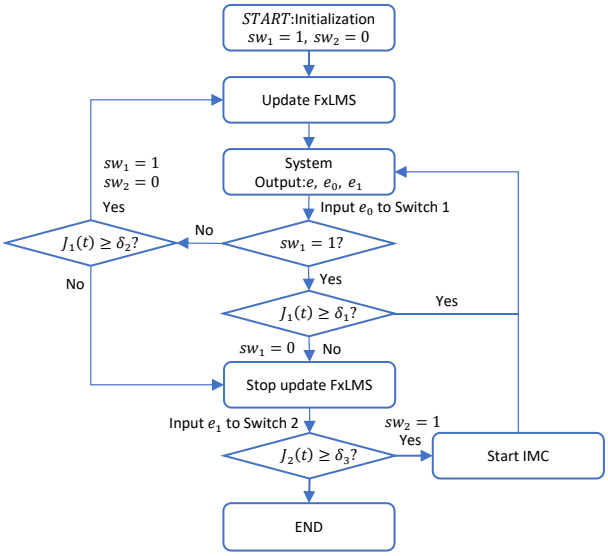

Fig. 4. The flowchart of IMC-LMS algorithm operation.

IV. Simulation And Experimental Results

As outlined in the introduction, feedback FxLMS algorithm [9] may lead to waterbed effect. We first showcase this phenomenon through numerical experiments. Specially, the noise source used in the simulation consists of a 100 Hz periodic disturbance combined with broadband noise spanning the frequency range of 250-290 Hz. The sampling rate of the simulation is 5 kHz. The key simulation parameters, μ and N, are set to 0.0002 and 8, respectively.

As illustrated in Fig. 5, the feedback FxLMS algorithm exhibits a waterbed effect during target frequency suppression,

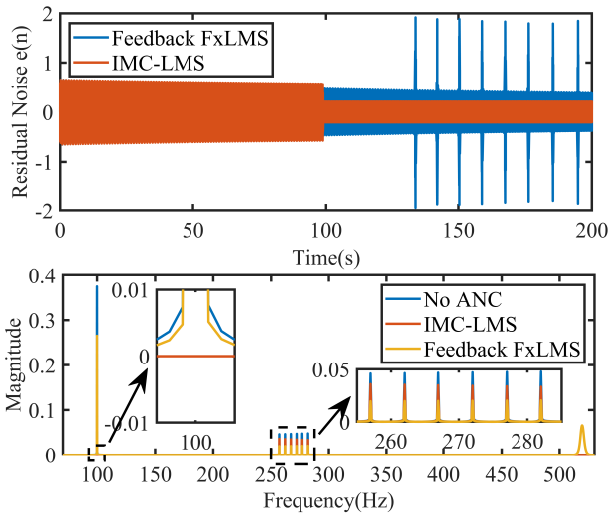

Fig. 5. The time domain and frequency domain performance between feedback FxLMS and IMC-LMS algorithms.

introducing unwanted noise at higher frequencies not present in the original noise source. This effect manifests as a noticeable "bulge" in the latter part of the time-domain noise reduction process. In contrast, the IMC-LMS algorithm effectively attenuates the target frequency while avoiding additional noise at other frequencies. These results highlight the superior stability and robustness of the IMC-LMS algorithm compared to the feedback FxLMS algorithm.

A. System Setup

In the experimental verification, our ANC test platform, depicted in Fig. 6, consists of a jamming speaker, a control speaker, power supply, amplifier, two microphones, sampling unit and computing equipment. In the test platform, the pipeline has two separate paths for processing noise signals and anti-noise signals. The noise speaker in the main path produces analog noise, while the control speaker produces an anti-noise signal in the secondary path.

The computational device is based on a cRIO-9049 NI 8-channel controller, equipped with a 1.60 GHz quad-core CPU, 4 GB DRAM, and 16 GB of storage, making it suitable for real-time control systems. The sampling unit employs an NI 9250 sound acquisition card with 2 channels and a synchronous sampling rate of 102.4 kS/s to capture the residual noise from the error microphone.

For all experiments in the sequels, the sampling frequency of the equipment was 5 kHz. The impulse response estimation of secondary channels was obtained by discrete identification using LMS algorithm $\hat{s}(n)$. The main parameters N, L are set to be 16, 1000 respectively. Additionally, the attenuation ability is quantified in decibels (dB) as $\text{Att} = 20\log_{10}(\frac{\text{Amp}_{\text{ANC on}}}{\text{Amp}_{\text{ANC off}}})$.

B. Composite Noise Cancellation

For the implementation, the composite noise used in the experiment consists of broadband noise ranging from 250 to 270 Hz, along with sinusoidal noise at 400 Hz for the first

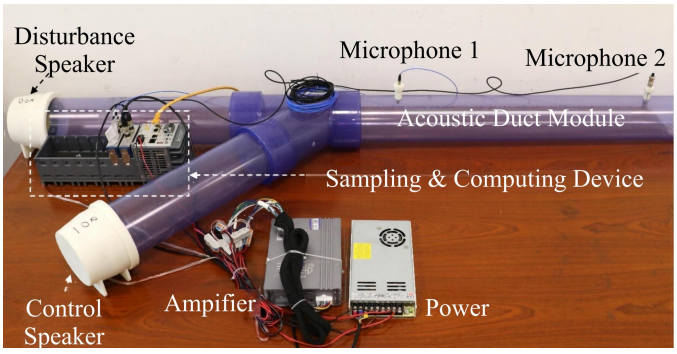

Fig. 6. The physical diagram of ANC test platform.

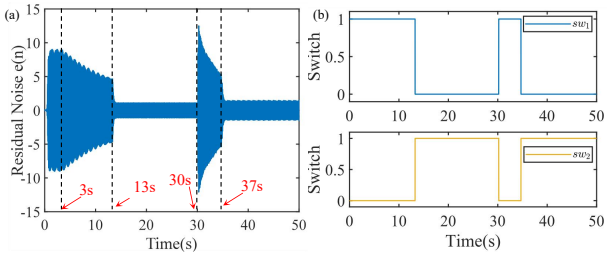

Fig. 7. Time history of residual error and switching signals of the proposed algorithm.

30 seconds. After 30 seconds, the noise mutates to be new composite noise including broadband disturbances between 280 and 300 Hz, along with the 400 Hz periodic component. The relevant parameters for the noise reduction algorithm, μ and g, are set to 0.00015 and 0.00004, respectively.

1) Convergence of the algorithm: Fig. 7-(a) shows the microphone data from the IMC-LMS algorithm under experimental conditions. At the beginning 3 seconds, the algorithm is inactive. During 3-13 seconds, the LMS algorithm undergoes its weight vector update process. At 13 seconds, the LMS update procedure terminates while the IMC algorithm initiates activation. The system converges quickly, with an attenuation of -18 dB. When the noise source changes at 30 seconds, both LMS and IMC algorithms sequentially update, achieving convergence around 37 seconds with an improved attenuation of -19 dB. This sequence demonstrates the system's ability to maintain noise suppression and achieve secondary convergence after sudden noise variations.

2) Adaptability in dynamic noise environments: Fig. 7-(b) illustrates the switching behavior of the IMP-LMS algorithm. At initialization, the switch signal $sw_1(n)$ is active and the switching signal $sw_2(n)$ is inactive. At 13 seconds, $sw_1(n)$ deactivates and $sw_2(n)$ activates, which implies the initiation of periodic signal suppression within the inner loop. At 30 seconds, $sw_1(n)$ reactivates and $sw_2(n)$ deactivates, followed by a third transition at 37 seconds, replicating the initial behavior. This experiment demonstrates the effectiveness of the switching mechanism in coordinating the inner and outer loop algorithms, ensuring stable noise suppression performance despite abrupt noise environment changes.

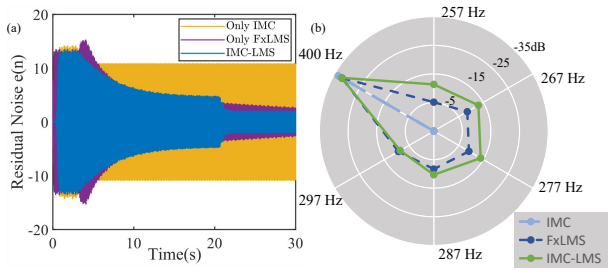

Fig. 8. SOTA comparison for composite noise. (a) time domain behavior of three methods. (b) the radar map for three methods.

TABLE I
SOTA COMPARISON RESULTS.

Method	Avg. Att (dB)	Convg. Time (s)
FxLMS	-13.9153	29.1346
IMC	-1.8981	**10.8457**
Ours	**-16.5861**	22.3819

C. SOTA Comparison

We compare our algorithm with the feedback FxLMS algorithm [8] and IMC algorithm [17] in the same noise environment. The noise source consists of broadband noise (250-300 Hz) and a 400 Hz sinusoidal signal. The noise reduction parameters μ and g are set to 0.00015 and 0.00003, respectively, with other parameters consistent with those in Section IV-A.

Noise Attenuation Efficacy: Fig. 8-(a) shows the time-domain noise reduction performance of the three algorithms. In Fig. 8-(b), the radar line extensions along the frequency axis represent attenuation (dB) at five broadband frequencies (257, 267, 277, 287, and 297 Hz), with the area indicated the composite noise cancellation capability across all frequencies. The IMC algorithm is unable to handle with broadband noise in the 250-300 Hz range but effectively suppresses the 400 Hz periodic signal. Although the feedback FxLMS algorithm demonstrates comparable performance to the IMC-LMS algorithm at certain frequency bands (e.g., 297 Hz and 400 Hz), its performance in other frequency regions is worse than the IMC-LMS algorithm. Table I shows the FxLMS algorithm's average attenuation of -13.9153 dB, lower than our algorithm's -16.5861 dB, with a longer convergence time for FxLMS. These results confirm the superiority and effectiveness of our approach.

V. CONCLUSION

We propose a novel hybrid active noise control (ANC) algorithm that effectively mitigates composite noise comprising low-frequency sinusoidal disturbances and broadband white noise. By introducing a switching mechanism to the filtered-x least mean square (FxLMS) algorithm, our approach leverages the benefits of FxLMS while eliminating its potential waterbed effect through the integration of internal model-based control. The robustness and effectiveness of the proposed method in addressing broadband noise, even in dynamic noise environments, are demonstrated through the development of an ANC verification platform. Although the algorithm currently achieves noise reduction at a single point, such as at the position of an error microphone, our future goal is to expand its application to spatial noise reduction, enhancing its impact across multiple locations in space.

REFERENCES

[1] B. Widrow and S. D. Stearns, *Adaptive signal processing*. Englewood Cliffs, NJ, USA: Prentice-Hall, 1985.
[2] S. M. Kuo and D. R. Morgan, *Active noise control systems: algorithms and DSP Implementations*. New York: Wiley, 1996.
[3] C. A. Jacobson, C. Johnson, D. C. McCormick, and W. A. Sethares, "Stability of active noise control algorithms," *IEEE Signal Processing Letters*, vol. 8, no. 3, pp. 74–76, 2001.
[4] S. Wang, H. Li, P. Zhang, J. Tao, H. Zou, and X. Qiu, "An experimental study on the upper limit frequency of global active noise control in car cabins," *Mechanical Systems and Signal Processing*, vol. 201, p. 110672, 2023.
[5] S. Kim and M. E. Altinsoy, "A complementary effect in active control of powertrain and road noise in the vehicle interior," *IEEE Access*, vol. 10, pp. 27 121–27 135, 2022.
[6] Y. Hinamoto and H. Sakai, "A filtered-x lms algorithm for sinusoidal reference signals—effects of frequency mismatch," *IEEE signal processing letters*, vol. 14, no. 4, pp. 259–262, 2007.
[7] I. T. Ardekani and W. H. Abdulla, "Theoretical convergence analysis of fxlms algorithm," *Signal Processing*, vol. 90, no. 12, pp. 3046–3055, 2010.
[8] D. R. Morgan, "History, applications, and subsequent development of the fxlms algorithm [dsp history]," *IEEE Signal Processing Magazine*, vol. 30, no. 3, pp. 172–176, 2013.
[9] L. Wu, X. Qiu, and Y. Guo, "A simplified adaptive feedback active noise control system," *Applied Acoustics*, vol. 81, pp. 40–46, 2014.
[10] L. Lu, K.-L. Yin, R. C. de Lamare, Z. Zheng, Y. Yu, X. Yang, and B. Chen, "A survey on active noise control in the past decade-Part I: Linear systems," *Signal Processing*, 2021.
[11] Y. Guo, D. Shi, X. Shen, J. Ji, and W.-S. Gan, "A survey on adaptive active noise control algorithms overcoming the output saturation effect," *Signal Processing*, p. 109525, 2024.
[12] F. Yang, Y. Cao, M. Wu, F. Albu, and J. Yang, "Frequency-domain filtered-x lms algorithms for active noise control: A review and new insights," *Applied Sciences*, vol. 8, no. 11, p. 2313, 2018.
[13] S. Skogestad and I. Postlethwaite, *Multivariable feedback control: analysis and design*. john Wiley & sons, 2005.
[14] L. Wu, X. Qiu, and Y. Guo, "A generalized leaky fxlms algorithm for tuning the waterbed effect of feedback active noise control systems," *Mech. Syst. Signal Process.*, vol. 106, pp. 13–23, 2018.
[15] L. Chen, N. Saikumar, S. Baldi, and S. H. HosseinNia, "Beyond the waterbed effect: Development of fractional order crone control with nonlinear reset," in *2018 annual american control conference (ACC)*. IEEE, 2018, pp. 545–552.
[16] D. Shi, W.-S. Gan, B. Lam, and K. Ooi, "Fast adaptive active noise control based on modified model-agnostic meta-learning algorithm," *IEEE Signal Process. Lett.*, vol. 28, pp. 593–597, 2021.
[17] P. Tomei, "Multi-sinusoidal disturbance rejection for discrete-time uncertain stable systems," *Automatica*, vol. 79, pp. 144–151, 2017.
[18] Y. Wang, G. Pin, A. Serrani, and T. Parisini, "Removing spr-like conditions in adaptive feedforward control of uncertain systems," *IEEE Transactions on Automatic Control*, vol. 65, no. 6, pp. 2309–2324, 2020.
[19] Y. Gong and Y. Wang, "A novel plug-and-play cooperative disturbance compensator for heterogeneous uncertain linear multi-agent systems," *IEEE Control Systems Letters*, vol. 8, pp. 2811–2816, 2024.
[20] T.-B. Airimitoaie, I. D. Landau, R. Melendez, and L. Dugard, "Algorithms for adaptive feedforward noise attenuation—a unified approach and experimental evaluation," *IEEE Transactions on Control Systems Technology*, vol. 29, no. 5, pp. 1850–1862, 2020.